Hydrology **2015**, *2*, 48-68; doi:10.3390/hydrology2020048

OPEN ACCESS

hydrology

ISSN 2306-5338

www.mdpi.com/journal/hydrology

Article

Assessment of Hydrogeochemistry and Environmental Isotopes in Karst Springs of Makook Anticline, Kurdistan Region, Iraq

Omed Mustafa [1,*], Broder Merkel [1] and Stephan M. Weise [2]

[1] Institute of Geology, Technische Universität Bergakademie Freiberg, Gustav Zeuner Str.12, 09599 Freiberg, Germany; E-Mail: merkel@geo.tu-freiberg.de

[2] Department Catchment Hydrology, Helmholtz Centre for Environmental Research-UFZ, Theodor-Lieser-Str. 4, 06120 Halle (Saale), Germany; E-Mail: stephan.weise@ufz.de

* Author to whom correspondence should be addressed; E-Mail: omedgeology@gmail.com; Tel.: +49-3731-39-2792; Fax: +49-3731-39-2720.

Academic Editor: Okke Batelaan

Received: 16 November 2014 / Accepted: 9 March 2015 / Published: 25 March 2015

Abstract: Karst springs of the Makook anticline were investigated to get more insight into the hydrogeologic, hydraulic, and hydrodynamic behavior of this complex karst system. Eight springs were studied in terms of hydrogeochemical constituents as well as $\delta^{18}O$ and $\delta^{2}H$ during September 2011 to November 2012. For the first time, the local meteoric water line was plotted for the area based on precipitation data from the period November 2011 to April 2012. The regional meteoric line plots between the global and Mediterranean meteoric water lines. The majority of the spring samples plot between the local and Mediterranean meteoric water lines implying influences by Mediterranean air masses, rapid infiltration of rainfall through the karst system and a short residence time (shallow karst aquifers). The correlation of *d*-excess and saturation index of halite was used to evaluate the evaporation process in karst waters of the area. The temporal variation in isotopic composition of karst springs was observed making it possible to distinguish between different origins for springs and indicate a possible connection between the aquifers and depending on this, the karst system can be classified into three aquifers: Behkme aquifer, Kometan aquifer, and Shiranish aquifer.

Keywords: karst springs; Bekhme; *d*-excess; environmental isotopes; local meteoric water line; Kurdistan Region

1. Introduction

Karst springs often discharge substantial amounts of water, which draws the interest of water resources researchers especially in arid and semi-arid areas facing water scarcity. Different methods and techniques were used by researchers to understand the response of the karst system to recharge events. Thermal patterns of karst springs were used by [1] as a key base for identifying two types of systems: thermally ineffective springs corresponding to rapid flow of event waters and effective thermal systems characterized by small fractures and slower water movements leading to equilibration of recharge and aquifer water's temperature. Electrical conductivity of karst waters may represent a good indicator to outline the flow system, whether it has a conduit or diffuse flow (retain piston flow). A piston flow phenomenon is the displacement of more mineralized water by intense rainfall recharge water toward the spring [2,3]. The hydrodynamic and hydrogeochemical characteristics together can outline the behavior of karst springs [2].

Karst springs of the Makook anticline represent the main source of water for drinking, agriculture, and other uses in the areas of Balisan and Akoyan, Kurdistan Region, Iraq. The population of villages and towns in the part of Ranya district in which the studied area is located comprised more than 20,000 inhabitants. Water demand in the area has increased sharply in the last 20 years because of the increase in population and their needs. The mountainous area with poorly developed infrastructure creates certain limitations for studying the area. Few works have been done in the field of isotopes in the area in recent years. Only two local meteoric water lines (LMWL) were determined in nearby areas. The LMWL for Haji Omaran area was extrapolated by Mawlood [4] from isotopic data of Halab station in Syria and Adana station in Turkey, and the meteoric water line of Basara area was published by Hamamin and Ali [5]. During 2000–2003 geologic and hydrologic investigations were carried out by a team from the Food and Agriculture Organization (FAO), including groundwater monitoring of Sarwchawa spring and wells in the area. Al Manmi [6] did an environmental isotopic study of surface and groundwater in Ranya area, which is close to the studied area and includes some of the springs considered in this work. According to [6], water of the Ranya area is of good quality with low salinity and thus suitable for drinking and irrigation purposes. Some possible recharge sources were determined depending on isotopic fingerprints. Karst aquifers in Makook system are mentioned as one thick Bekhme aquifer, which, according to [6,7], may contain Bekhme, Qamchuqa, and Kometan Formations. Bekhme aquifer consists of highly fissured, well-karstified carbonate rocks containing many caves and channels.

The objective of this study is to explore the applications of environmental isotopes of $\delta^{18}O$ and $\delta^{2}H$ in the field of karst springs. This work includes an attempt to build a local water line for the area, which had not done before. The local meteoric water line was correlated to the regional lines to investigate the source and determine the residence time of this water till it reaches the springs. This study also addresses the relation between hydrodynamic and hydrogeochemical characteristics of the karst springs.

2. Study Area

2.1. Geography

The area of interest is located in the Kurdistan region in the northeast of Iraq, mainly in Sulaimani governorate, Ranya district (Figure 1). The area is situated within latitudes 36°10′–36°35′ north and longitudes 44°30′–44°50′ east in the elevation range of 500 to >2000 meter (m) above sea level (a.s.l).

Makook Anticline Mountain lies in a northwest–southeast direction and is surrounded by Shawre valley in the northeast and Balisan valley in the southwest. The area of interest comprises about 400 km^2 and is part of the Dokan lake catchment.

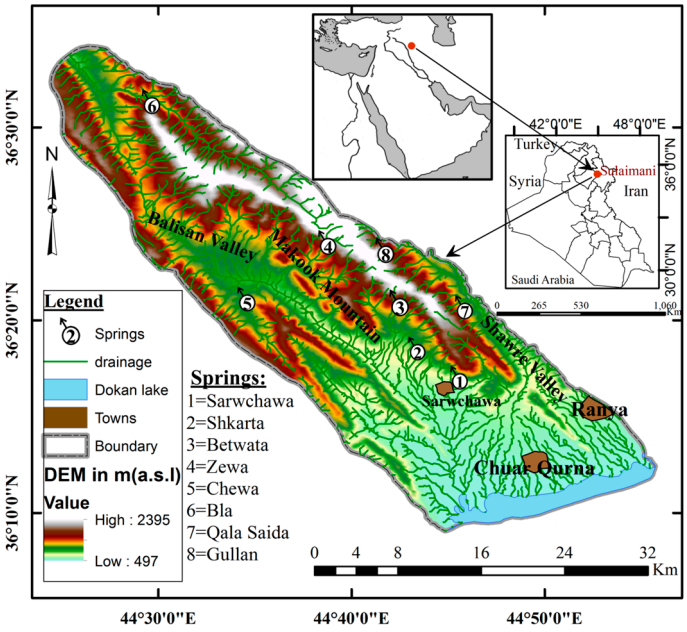

Figure 1. Digital elevation model (DEM) showing the area of interest in Kurdistan Region, Iraq. Numbers 1 to 8 refer to the springs where sampling was conducted.

The studied area is characterized by humid to moist climate. Rainy season starts from October and mainly ends in May (with minor showers in June, July, and September). The mean annual climatic parameters are presented in Figure 2 for the period 1980 to 2012. The highest precipitation rate, highest relative humidity, and lowest temperature are observed in February. The mean annual rainfall for the mentioned period is 570.5 mm and the average annual temperature is 20 °C. The mean annual evaporation (pan) is about 2000 mm and the mean relative humidity is about 47% [8].

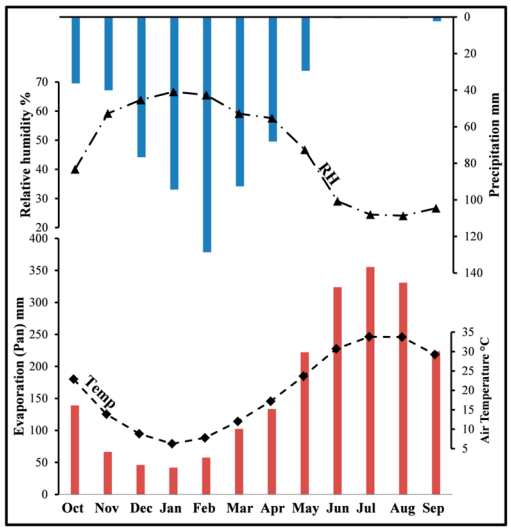

Figure 2. Climatological data of the Dokan Meteorological Station (690 m a.s.l) located in the investigation area. Averages for the period 1980–2012 are shown [8].

2.2. Geologic Setting

Rocks of Mesozoic and Cenozoic age can be found in the region of interest (Figure 3). Two units of Jurassic rocks are cropping out, representing older rocks: (I) Sarki and Sehkaniyan formation, which are composed mainly of limestone, dark dolomite, and shale [9]; and (II) Sargelu formation (Bajocian–Bathonian), Naokelekan formation (Late Oxfordian–Early Kimmeridgian), Barsarin formation (Kimmeridgian–Early Tithonian), and Chia Gara formation (Late Tithonoan), which include bedded to massive dolomite, limestone, bituminous limestone, and marl. The Cretaceous unit comprises Balambo and Sarmord formation (marly and bedded limestone, bedded dolomite, and marl), Qamchuqa formation (mainly massive limestone and dolomite), Bekhme formation and locally Kometan formation (well bedded to massive limestone), Shiranish formation (well bedded limestone and marl), and Tanjero formation (sandstone, claystone, and conglomerate) [10]. Kometan formation does not appear in the geological map (Figure 3), while it is more regional map and the existence of Kometan formation was in time of map creation still suspicious. Near Sarwchawa town, Kometan formation changed laterally to Bekhme formation through a transitional zone [11], and both formations are possibly overlain by Shiranish formation. Jurassic and Cretaceous rocks are occasionally overlain by Quaternary fan deposits (boulders, gravel, and fine clastics) and a thin layer of soil (mainly in the valleys, because of soil erosion in that mountainous area).

Makook Anticline represents a double plunging anticline (NW–SE) within in the parallel trend of Zagros folded structures between Ranya and Palawan anticlines and Sahwre and Balisan synclines (in between) in the NE and SW, respectively (Figure 3). The area is characterized by tectonic distortion, especially in the northwest part of Makook Anticline.

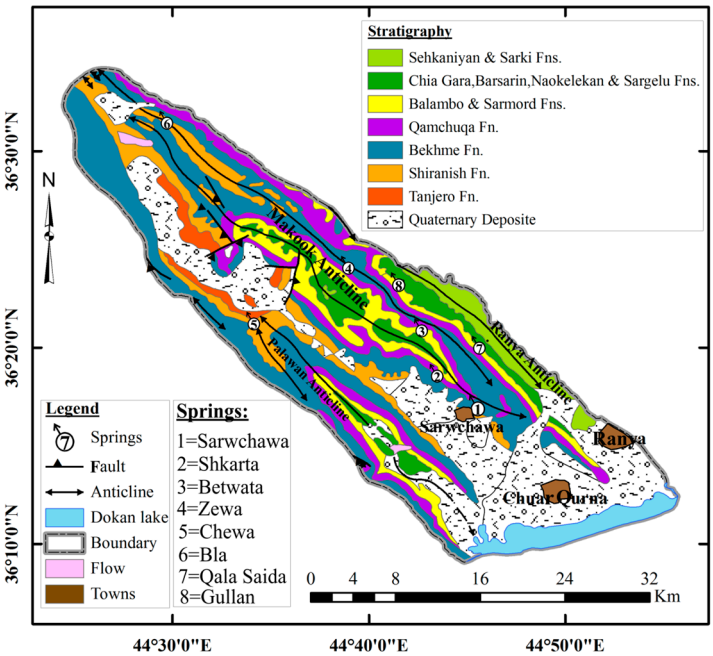

Figure 3. Geological map of the area (modified from [12]). Numbers 1 to 8 refer to the springs where sampling was conducted.

2.3. Hydrogeology

Generally, all springs are within the Makook Anticline Mountain, except Chewa spring, which is located in the Balisan valley. Two main Karst aquifers are recognized in the region of interest. First, Bekhme karst aquifer supplies major springs along Makook anticline, including Zewa, Chewa, Bla, and Gullan springs (Figure 3). Bekhme aquifer is distinguished as a well-karstified, thick, semi-confined aquifer underlain by Sarmord formation (aquiclude). The second one is Kometan formation, which represents the source of Sarwchawa and Betwata springs. Kometan formation is a well-karstified, highly fissured aquifer with confined to semi-confined conditions and overlain by Shiranish formation [7]. The aquifer is composed of carbonate rocks and contains a large amount of groundwater, varying in space and time. Strong karstification cycles took place in the aquifer system during the Paleocene–Miocene period [13]. It is assumed that karstification happens recently. One of the springs (Shkarta) drains poorly developed karst (with small fissures). This spring is located in the Shiranish formation (marl and marly limestone), which was inconsistently recognized as a fissured aquitard (locally in the marly limestone part) by [6]. The existence of Qamchuqa formation aquifer in studied area is possible, as mentioned by [6], but no field evidence has been observed.

3. Methodology

Eight karst springs (Sarwchawa, Shkarta, Betwata, Zewa, Chewa, Bla, Qala Saida, and Gullan) were monitored and sampled during six periods (September 2011, December 2011, April 2012, June 2012, September 2012 and November 2012). Precipitation samples (two snow and eight rain samples) were collected between November 2011 and April 2012 from three locations near Ranya town, Qala Saida and Gullan springs. Precipitation samples were collected by rain collector non-systematically depending on precipitation events. Field parameters (pH, conductivity and water temperature) were measured on-site (springs outlet). Redox potential (Eh) was measured via a WinLab redox meter (Windaus Labortechnik, Germany) and WTW SenTix-ORP electrode (WTW: a Xylem Group brand, Germany) and checked by standard redox buffer (pH = 7 and 220 millivolts at 25 °C). The parameters pH, electrical conductivity (EC), dissolved oxygen (DO) and water temperature (T) were measured on-site using a multi-parameter WTW model 3430, WTW pH electrode SenTix-940, WTW TetraCon-925 conductivity electrode and WTW FDO-925 optical dissolved oxygen sensor. Three-point calibration was carried out for the pH electrode via technical WTW buffers (pH = 4.01, pH = 7 and pH = 10). The EC electrode was checked with WTW standard control solution; settings were chosen so that the output of the electrode was converted to a water temperature of 25 °C. The optical sensor for dissolved oxygen measurement was checked regularly using a water vapor saturated air vessel. A certified mercury-thermometer was employed for air temperature measurement. Alkalinity was determined immediately after sampling by means titration and converted to hydrogen-carbonate (HCO_3^-) according to [14]. Because no continuous discharge measurements of the springs were available, different methods (velocity–area using current meter and volumetric readings) were employed to record the discharge of the springs during the monitoring period from September 2011 to November 2012. Due to difficulties in the field, flow measurements and field parameters were measured

only six times (September 2011, December 2011, April 2012, June 2012, September 2012 and November 2012) accompanying the sampling processes (Table S1).

All samples were filtered by 0.2 µm filters and stored at 4 °C until analysis in the laboratory. Samples analyzed by ICP-MS were acidified with an ultra-pure 1:1 nitric acid (30% HNO_3) mixture after filtration in the field. Batches of 48 samples were analyzed in the laboratories of the Chair of Hydrogeology, Technische Universität Bergakademie Freiberg, Germany. Lab work included determination of Si and Sr ions with an ICP-MS XSeries-2 model (Thermo Scientific, Bremen, NS, Germany). Major cations Ca^{2+}, Mg^{2+}, Na^{+}, K^{+} were determined by ion chromatography (IC) using an 850 Professional IC Metrohm (Switzerland) and Metrosep C4-150 column with 2 mM dipicolinic acid eluent. Major and minor anions F^{-}, Cl^{-}, PO_4^{3-}, SO_4^{2-}, Br^{-}, and NO_3^{-} were determined by a Metrohm Compact IC Pro 881 (Switzerland) and Metrosep A sup 15–150 column with 3 mM $NaHCO_3$ and 3.5 mM Na_2CO_3 eluent. The reproducibility of IC and ICP-MS determination were less than 2% and 5%, respectively. Stable isotopes of oxygen ($\delta^{18}O$) and deuterium ($\delta^{2}H$) were determined by means of an LGR liquid-water isotope analyzer-DLT 100 (ABB Company, Mountain View, CA, USA) with a precision of <0.1‰ for $\delta^{18}O$ and <0.3‰ for $\delta^{2}H$.

The ion balance, saturation index of calcite ($SI_{Calcite}$), dolomite ($SI_{Dolomite}$), gypsum (SI_{Gypsum}), fluorite ($SI_{Flourite}$), halite (SI_{Halite}), celestine ($SI_{Celestine}$) and partial pressure of CO_2 (P_{CO2}) in the spring samples were calculated by means of PHREEQC [15] with the WATEQ4F database.

Non-parametric two-tailed correlation analysis (Kendall and Spearman correlations) was performed for the hydrogeochemical and field parameters in addition to basic statistical treatment using SPSS software package.

4. Results and Discussion

Hydrologic and hydrochemical data of the Makook Karst springs are shown in the electronic Tables S1 and S2. The hydrochemical data were assessed by PHREEQC [15]. The relative analytical error (E%) of the most samples was within an acceptable range of ±2%, except Shkarta and Zewa springs, which have a higher deviation in April 2012 and September 2012, respectively, but generally the accuracy is acceptable (Table S2).

4.1. Discharge and Recharge Estimations

From the discharge of springs, mean annual precipitation, catchment area, and average chloride concentration in precipitation and groundwater, different hydrologic parameters were estimated. Maximum discharge of karst springs has an important impact on hydrological modeling [16]. The maximum estimated discharge (D_{me}) for an area is defined as:

$$D_{me} = P \times A_c \quad (1)$$

where P is mean annual precipitation in mm and A_c is catchment area in square meter (m^2). The mean annual precipitation is 570.5 mm (1.81×10^{-5} L/m^2/s) and the studied area is 4×10^8 m^2; therefore D_{me} of the studied karst area is 7240 L/s.

The recharge in the area of interest was estimated using two methods: chloride mass-balance (CMB) and empirical Kessler method. The CMB method has often been used for recharge estimation [17,18]

and is applicable in semi-arid regions when additional sources of chloride are absence [19,20]. The precipitation in the area of interest was sampled 10 times during hydrological year (2011–2012). The temporal variation of chloride seems to be rather low (Table 1). Thus it is assumed that this average can be used for recharge calculation. Most of the chloride in the karst water is from precipitation (about 0.08 meq/L). Only 0.7% (0.02 meq/L Cl) of the chloride in karst waters stems from carbonate rocks, except in Shkarta spring where the chloride concentration is about 0.2 meq/L by the interaction of water with clay minerals of Shiranish aquifer (Tables 1 and S2). Most of the recharge areas of the springs are not arable land (except some areas related to Sarwchawa and Shkarta springs). Therefore fertilizers as additional source of chloride were excluded. Surface runoff in the recharge area of the springs is not significant and can thus be omitted from the recharge estimation. Recharge (R) in the area of interest was estimated by the CMB method:

$$R = P \times (Cl_p/Cl_{sp}) \quad (2)$$

where Cl_p is average reference chloride concentration in precipitation and Cl_{sp} is average chloride concentration in spring water (both in mg/L). The re-calculation of Cl in precipitation to reference Cl is to consider the impact of evapotranspiration on the mass-balance estimation. The average reference Cl of precipitation is 2.52 mg/L and the average Cl in studied springs is equal to 2.9 mg/L, thus the estimated recharge is 496 mm/year. The recharge estimation by Kessler's method [21] was originally adapted for karst aquifers in semi-arid regions, and is based on the pluviometric data of last four months of the year. The estimated recharge in the area of interest by Kessler method is equal to 525 mm/year (the methodology of recharge calculation is described in [21]).

Table 1. Isotopes, altitude, and hydrochemistry of precipitation.

Sample	Date of	$\delta^{18}O$		δD		*d*-Excess	Altitude	T_{Air}	*Evap.*	*Precip.*	pH	Cl	Na
Code	Sampling	‰	*StD*	‰	*StD*	‰	m.a.s.l	°C	mm	mm		(mg/L)	(mg/L)
R-1	25.11.11	−5.18	0.05	−23.07	0.34	18.4	882	11	1.4	0.2	6.3	1.9	0.41
R-2	31.12.11	−9.18	0.08	−52.8	0.16	20.6	882	8.5	1.4	12.5	6.5	3.2	0.2
R-3	18.01.12	−3.35	0.08	−1.95	0.29	24.8	882	7.5	0.6	9	6.2	2.4	0.1
R-4	31.01.12	−12.29	0.07	−82.31	0.18	16	882	7.5	1	45	6.3	2.8	0.17
R-5	07.02.12	−7.91	0.11	−44.95	0.52	18.3	882	7	2	20.2	6.1	1.9	0.06
R-6	18.02.12	−9.5	0.12	−57.6	0.57	18.4	882	8.5	2.1	9	6.4	2.5	0.43
R-7 *	18.02.12	−8.27	0.08	−39.17	0.27	27	1460	8.5	2.1	9	6.3	2.5	0.7
R-8	02.04.12	−9.27	0.08	−54.57	0.38	19.6	882	7.5	1.1	15	6.5	2.4	0.76
R-9 *	04.04.12	−10.66	0.03	−55.77	0.25	29.5	845	3.5	1.3	25	6.5	2.3	0.22
R-10	15.04.12	−5.38	0.04	−28.85	0.24	14.1	845	12.5	4.3	29	6.5	4.2	0.43

StD = Standard deviation; ***** = snow samples; T_{Air} = Air temperature; ***Precip.*** = Precipitation; **Evap**. = Evaporation; Meteorological parameters represents mean daily values of the sampling date.

The recharge rate according to Kessler's estimation is 92% and of CMB is 87%. The difference between the two estimations is normal (being different approaches were used), but the latter is more reasonable depending on the field observation, and conclusions of [22] in karst systems of other semi-arid region. These estimations are convenient with the calculated effective recharge (R_E) that defined as:

$$R_E = (D_{sp}/D_{me}) \times 100 \quad (3)$$

where R_E is the effective recharge (the amount of water that reach the groundwater), D_{sp} is the total average discharge of the springs (4037 L/s), and D_{me} is maximum estimated discharge. The effective recharge in the studied area is 55.8%, and depending on these estimations it can be assumed that minority of the precipitation will loss by evaporation and transpiration.

4.2. Springs Hydro-Chemograph Analysis

Relating to the hydro-chemographs, different interpretations for the studied springs can be concluded (Figure 4). Flow rates in the springs (discharge) of the study area vary according to the capacity of the aquifer and degree of karstification in the spring aquifer (Figure 4a and Table S1). The Sarwchawa spring shows higher flow rates (2370 and 4630 L/s in dry and rainy seasons, respectively) and represents the most developed karst spring in the Makook karst system. The Shkarta spring (Shiranish formation) represents the less developed karst or non-karst spring with a low flow rate of 0.75 L/s, originating from fissured marly limestone [6]. Sarwchawa, Shkarta and Qala Saida springs show a direct response of increasing discharge with respect to October 2011/April 2012 precipitation events (Figure 4a,b). In Shkarta spring, the response of discharge to the recharge events is less compared to the majority of the springs. As results of low flow rate in marly rocks, the residence time then will be high [23]. Therefore, low flow rates in micro-fissures of Shiranish marly limestone can be the reason of high residence time and gradually varied discharge confirms this hypothesis. Betwata, Zewa, Chewa, Bla and Gullan springs show a nearly two months delay (maximum peak discharge appear in June 2012). The hydrograph of Betwata spring shows two peaks in response to the October–December 2011 and April–June 2012 rainfall events. A similar pattern can be noticed in Chewa spring's pattern but with lesser response to the October/December 2011 raining event. A gentle rise in Zewa spring's hydrograph was recorded and a steep decrease of discharge was recorded, which refers to a low storage capacity in the karst aquifer that feeds Zewa spring. Decrease in Bla's hydrograph in the December 2011 rainfall event was observed, which makes this spring different from all other studied springs.

The pH of the springs ranges between 7.1 and 8.4 (average 7.5) showing neutral to slightly alkaline water (Figure 4b and Table S1). The variability in pH of the springs is caused by changes in flow paths, water discharge, and residence times within the aquifer [24]. Two of the springs (Zewa and Gullan) show decrease in pH during the December 2011 precipitation event. The similarity in pH patterns refers to the similarity in origin of water (same aquifer). The other springs show increasing of pH within the same recharge event (December 2011 precipitation). The addition of the newly recharged precipitation (December 2011–April 2012) caused an obvious decrease in pH of all the springs, and this was repeated in the November 2012 precipitation event. The pH value of precipitation collected during the current study indicates slightly acid conditions (Table 1). According to the nature of the karst aquifer, different impacts of this acidic recharged water are expected. Therefore, temporal variation in pH value can be used as a tracer in karst waters.

The redox potential of the springs showed partially oxidizing waters (323–478 mV, with an average of 383 mV). Chemistry of the karst waters in the unsaturated zone is modified by local flow variations and changes in redox condition [25]. Analysis of the redox graphs reveals a falling pattern of Eh for all

springs (Figure 4c). Variation of Eh graphs is controlled by changes in karst water temperature, and this relation is more significant in Shkarta, Chewa, Bla and Gullan springs. The increasing of Eh in Shkarta, Betwata, Chewa and Bla springs can be interpreted as a result of recharge with water containing more oxygen [26] in a shallower depth compared with the first group of springs.

Electrical conductivity ranges between 265 and 1117 µS/cm outlining differences in recharge rate and seasonal effects between wet and dry periods (Figure 4d). Generally, conductivity decreases in wet seasons, reflecting dilution by precipitation water. But this situation became completely the opposite (except Zewa and Gullan springs) during the November 2012 precipitation event when EC increases drastically during dilution by recharge. The dilution processes followed by a piston flow effect assumed to be the reason of the EC increase during the recharge period [3].

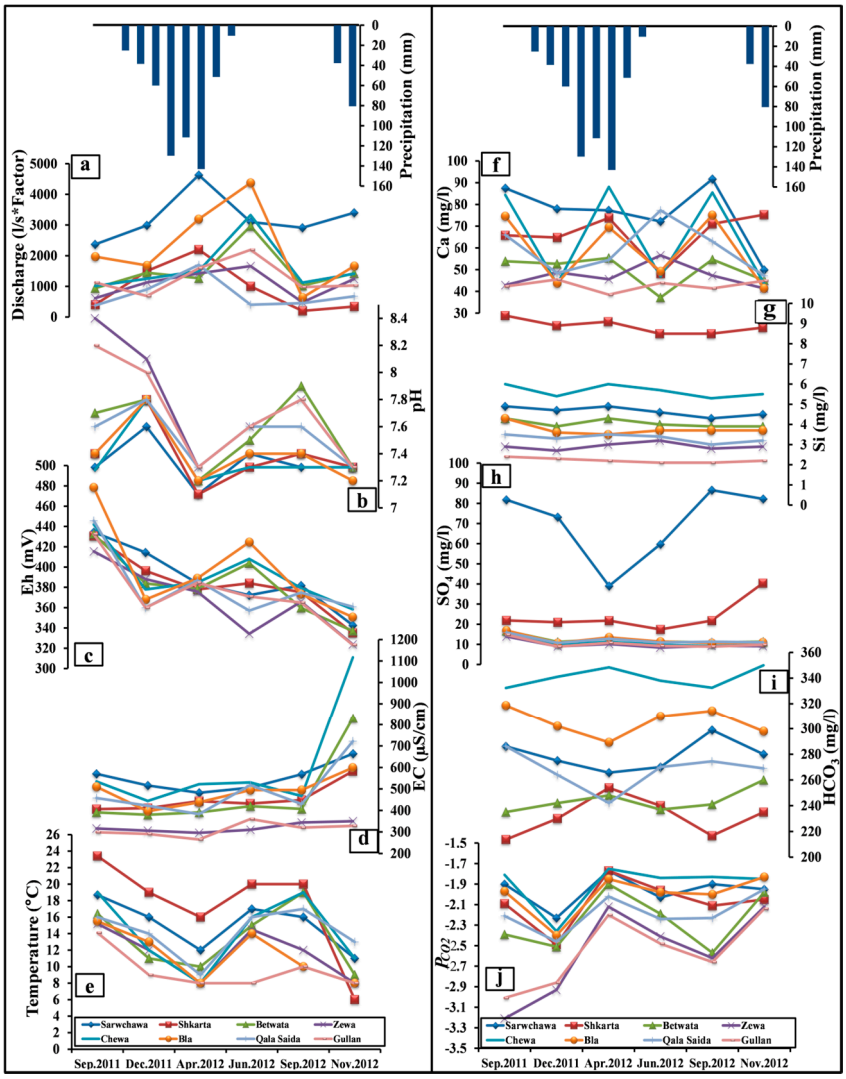

Figure 4. Hydro-chemograph of the karst springs. The recorded precipitation is from September 2011 to November 2012 period. (**a**) Hydrograph; discharge values were multiplied by a factor because of the differences in the magnitude and to better magnify their response to precipitation as follow: Sarwchawa × 1, Shkarta × 2000, Betwata × 50, Zewa and Chewa × 10, Bla × 5, Qala Saida × 250 and Gullan × 25; (**b**) pH; (**c**) Eh; (**d**) EC; (**e**) water temperature; (**f**) Ca; (**g**) Si; (**h**) SO_4; (**i**) HCO_3; and (**j**) P_{CO2}.

The water temperature of the springs ranges between 6 °C and 23.4 °C (Table S1). The water temperature pattern in Shkarta spring was like that of Sarwchawa spring, but with higher amplitude in Shkarta (water temperature variation: 17.7 °C), which was recorded as the maximum among the springs studied (Table S1). A lateral groundwater influx from one aquifer to another with presence of clay and marl layers in the vicinity of springs leads to mixing and causes a decrease in water temperature [27]. This scenario is the reason for the drastic decrease of spring water temperature (as obvious in the thermal pattern of Shkarta spring) in the rainfall period of October–November 2012 (Figure 4e). According to the stratigraphic superposition, a lateral influx of water from Kometan aquifer to Shiranish aquifer assumed to be the reason of the October–November 2012 temperature decrease in the Shkarta spring. The water temperature pattern in Betwata is the same as in the two former springs, but with nearly two-month time lag until recovery. The time lag in temperature recovery in karst springs results from low transit times, low development in karstification, and diffuse flow pattern [3]. The variability of temperature in karst springs is considered a tracer for recharge and geometry of the aquifer [1]. Slow movement of recharge water through Sarwchawa and Gullan spring aquifer results in thermal equilibrium between recharge and discharge water and indicates long residence time and rather deep karst. The enrichment of Sarwchawa spring water with Ca, Mg and SO_4 indicates higher residence time, more intense water-rock interaction, and slower movement of recharged water through the aquifer. Gullan spring shows smoother thermal fluctuation at lower temperature (8 °C–14.1 °C) compared to Sarwchawa (11 °C–18.7 °C), which may be caused by differences in altitude of the springs outlet, elevation of recharge area, flow type, and depth of the aquifer (lower altitude, deeper aquifer and conduit flow for Sarwchawa spring). There is some evidence that convective heat transport of infiltrating water (recharge) is responsible for the observed temperature patterns [28]. Unfortunately the data given are not sufficient to calculate the recharge by inverse modeling of the temperature distribution in the aquifer over time.

Temporal variation of major cations (Ca^{2+} and Mg^{2+}) and anions (SO_4^{2-} and HCO_3^-) between wet and dry periods correlates to corresponding precipitation events (September 2011 to September 2012) and EC as illustrated in Figure 4. The calcium chemographs of spring water mainly show decreasing calcium concentration during recharge periods, except Zewa spring (Figure 4f), which shows the reverse (increasing Ca concentration with increasing recharge). Similar decreasing of Ca through dilution by low mineralized recharge water was reported by Vesper and White [29] for karst springs in Kentucky, USA. A zigzag-like pattern in Ca chemographs of Chewa and Bla springs was observed and indicates the similarity in recharges and flow systems for both springs. A time lag was enhanced by the most noticeable changes in hydrogeochemistry after the recharge events. This time lag suggests the presence of piston phenomena [29].

Chemograph of Si shows low variation, implying that silica in karst waters is conservative (Figure 4g). Shkarta spring shows higher Si concentration compared to the other springs, indicating presence of silicate mineral in this aquifer (Shiranish marly limestone).

Sulfate concentrations show the same variation as Ca corresponding to the dilution with recharge water, except in Zewa and Gullan springs, which showed the opposite patterns (Figure 4h). The sulfate concentration is higher in Sarwchawa spring. Sulfate-rich waters may form by oxidation of pyrite in carbonate rocks [30]. Oxidation of pyrite concretions [9,31,32] and gypsum impurities along the flow path of Kometan aquifer leads to formation of this sulfate rich water. The direct response of sulfate to

recharge is interpreted as presence of conduit type of flow and is reported from different karst springs worldwide [29,33–35].

A general trend of increasing P_{CO2} with increasing discharge was observed in the karst springs. This reflects the decrease of diffuse atmospheric CO_2 and increase of CO_2 in soil [36]. The pattern of P_{CO2} in karst springs is consistence with sulfate patterns rather than the Ca ones (Figure 4j). Increasing of P_{CO2} is accompanied by increasing of Ca, sulfate, EC, T and Eh.

4.3. Water–Rock Interaction and Geochemical Processes

The variation in hydrochemistry of water can be used as an indicator to understand water–rock interactions and geochemical processes during flow in the aquifers [37]. In order to identify the hydrochemical type of the spring waters different techniques were used. Karst waters were classified depending on the relative abundance of Ca^{2+}, Mg^{2+}, Na^{+}, and K^{+} as major cations and HCO_3^{-}, SO_4^{2-}, Cl^{-}, and NO_3^{-} as major anions (in meq/L). According to the abundance, all springs in all sampling periods were classified as Ca-HCO_3 water except Sarwchawa spring, which was classified as Ca-HCO_3-SO_4 water. The excess of Ca and SO_4 in Sarwchawa spring relates to the longer residence time. A Chadha diagram classification [38] was also used for classifying the spring water, and all springs show Ca-Mg-dominant-HCO_3 type (5th-sub field), which indicates that alkaline earths and weak anions exceed both alkali metals and strong anions.

Different hydrogeochemical relations indicate different sources of geologic material for the karst waters of the area (Figure 5). The significant relations of Na–Cl and Na–(NO_3 + PO_4) refers to different aquifers and sources of geochemical materials in addition to meteoric water (Figure 5a,b). Up to 0.017 meq/L of sodium stems from rainwater, while 0.093 of Na stems from limestone and dolomite of Kometan and Bekhme formation. Excess Na in karst water stems from clay minerals and feldspars [39]. Therefore clay minerals of Shiranish marly limestone seem to be the source of excess Na in water of Shkarta spring. According to this variety of sources of geochemical materials, three different aquifers were recognized in the karst system of Makook anticline. (1) Springs feed by Shiranish aquifer (marly limestone) are characterized by high Na, Cl, NO_3 and PO_4; (2) springs feed by Kometan aquifer (limestone) shows medium content of Na, Cl, NO_3 and PO_4; and (3) springs feeds by Bekhme aquifer (dolomite) characterized by lower Na, Cl, NO_3 and PO_4 compared to the other aquifers (Figure 5a,b).

Calculated saturation indices (Table S3 and Figure 5c) indicate that Zewa, Chewa and Qala Saida springs are over-saturated (SI $\geq$ 0.05) with calcite while Sarwchawa, Shkarta, Betwata and Bla springs are in equilibrium ($-0.05 \leq$ SI ≤ 0.05). De-dolomitization processes are in progress in waters in equilibrium with calcite and under-saturated with dolomite [40]. Only Gullan spring was under-saturated (SI ≤ -0.05) with respect to calcite, which suggests shorter flow path and residence time in the aquifer compared to the other springs (Figure 5c). Regarding the $SI_{Dolomite}$, only Qala saida spring was in equilibrium, and the rest were under-saturated with respect to dolomite. All springs were under-saturated with respect to gypsum, fluorite, and halite. Dissolution is assumed to be incongruent if a mineral dissolves while another one is oversaturated and thus precipitate. Obviously, incongruent dissolution occurs in waters of Sarwchawa, Shkarta, Betwata and Bla springs. SI_{Gypsum} is significantly correlated with $SI_{Celestine}$ (Figure 5d) indicating presence of gypsum and celestine ($SrSO_4$) impurities in karst rock, especially in springs drained from limestone. The sources of Sr are controlled by the stratigraphy [41] as

well as the lithology. Thus, limestone of Kometan formation provides the karst water with more Sr than the two other aquifers (Figure 5d).

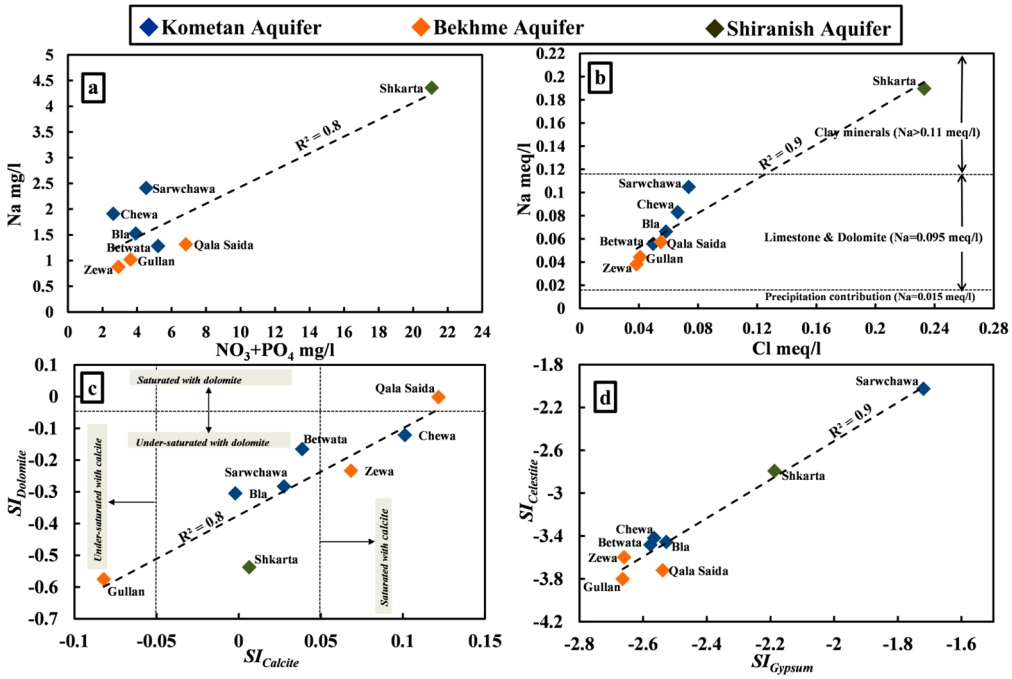

Figure 5. Hydrogeochemical relations among karst waters. (**a**) Na–(NO_3 + PO_4) plot, (**b**) Na–Cl plot, (**c**) $SI_{Calcite}$ *vs.* $SI_{Dolomite}$ and (**d**) SI_{Gypsum} *vs.* $SI_{Celestine}$; concentrations of Na and Cl in rainwaters are mean values from 10 precipitation samples, which are listed in Table 1.

A nonparametric Kruskal-Wallis-H test was performed to test the significance of the above grouping. The data were taken randomly and independently of each other. The results confirm that the three groups of spring water are different by means of *p*-value ≤ 0.05 for Ca, Mg, Na, K, Cl, SO_4, HCO_3, F, NO_3, Si and Sr, except PO_4, which shows higher *p*-values.

4.4. Isotopes in Precipitation and Karst Springs

4.4.1. Development of a Local Meteoric Line

Oxygen ($\delta^{18}O$) and hydrogen ($\delta^{2}H$) isotope compositions for the precipitation and spring samples are given in Tables 1 and 2, respectively. The isotopic composition of precipitation in the studied area ranged between −12.28 to −3.35‰ for $\delta^{18}O$ and −82.3 to −1.95‰ for $\delta^{2}H$. The regression equation of the LMWL is $\delta^{2}H‰ = 20‰ + 7.9 \times \delta^{18}O$ ($R^2 = 0.95$, $p \leq 0.001$, and $n = 10$). In relation to the Global Meteoric Water Line (GMWL), given by equation $\delta^{2}H = 10‰ + 8 \times \delta^{18}O$ [42], and the Mediterranean Meteoric Water Line (MMWL), given by equation $\delta^{2}H‰ = 22‰ + 8 \times \delta^{18}O$ [43], the LMWL is located between these two (Figure 6), and it is closer to MMWL. The LMWL of the studied area is very close to that of Haji Omaran area (50 km northeast of the studied area, 36°40′00″N, 45°03′00″E and with higher altitude) $\delta^{2}H‰ = 20‰ + 8 \times \delta^{18}O$ [4], but far away from that of Basara area (100 km southeast of the studied area, 35°20′30″N, 44°57′40″E and with lower altitude) $\delta^{2}H‰ = 14.4‰ + 7.7 \times \delta^{18}O$ [5]. The *d*-excess higher than 20‰ in precipitation results from arid vapor sources [44]. The vapor sources of some precipitation samples (R-2, R-3, R-7, and R-9) are arid (low humidity), because the *d*-excess is

higher than 20‰. The evaporation of precipitation can reduce the *d*-excess [44]. Therefore, the *d*-excess in samples R-1, R-4, R-5, R-6, R-8 and R-10 was reduced as a result of water loss by evaporation (Table 1). A continental effect is a possible reason for the high *d*-excess in some precipitation samples (R-3, R-7 and R-9), because they were higher than that of the MMWL. Another possible reason for this high *d*-excess in R-7 and R-9 is the origin and nascence condition [45], because they represent snow samples.

4.4.2. Factors Affecting Stable Isotopes in Precipitation

The air temperature is correlated with *d-excess* (*d-excess* ‰ = 31.9‰ − 1.4‰/°C × T_{Air} (°C), R^2 = 0.67, p = 0.03, n = 10). This correlation may emphasize the seasonal effects and thermodynamic conditions in the atmosphere [45,46] (Figure 7a) and may also be underlined by the increase of evaporation with temperature (Evaporation (mm) = 0.26 mm/°C × T_{Air} (°C) – 0.44 mm, R^2 = 0.6, p = 0.05, n = 10). The amount effect (Figures 8 and 9b) shows a negative correlation (higher rain amount shows a lower isotopic signature), which was reported worldwide except in polar areas [47].

Table 2. Isotopic composition of spring water samples.

Sample Code	$\delta^{18}O$ ‰							$\delta^{2}H$ ‰							*d*-Excess
	2011		2012					2011		2012					
	15-Sep.	6-Dec.	26-Apr.	4-Jun.	5-Sep.	11-Nov.	Mean ‰	15-Sep.	6-Dec.	26-Mar.	4-Jun.	5-Sep.	11-Nov.	Mean ‰	(Mean) ‰
Sarwchawa (1)	−7.42	−7.63	−7.47	−7.41	−7.51	−7.59	−7.42	−39.91	−40.02	−39.18	−39.2	−39.81	−43.39	−40.25	19.8
Shkarta (2)	−6.27	−6.42	−6.26	−6.14	−6.26	−6.18	−6.25	−32.33	−32.35	−32.7	−31.9	−32.43	−35.57	−32.88	17.1
Betwata (3)	−7.8	−7.85	−7.68	−7.74	−7.73	−7.79	−7.77	−40.95	−40.42	−40.39	−40.92	−40.56	−43.87	−41.18	20.9
Zewa (4)	−8.29	−7.98	−8.07	−8.1	−8.19	−8.08	−8.12	−43.57	−42.79	−43.14	−44.03	−43.59	−45.93	−43.84	21.1
Chewa (5)	−7.67	−7.4	−7.91	−7.51	−7.69	−7.66	−7.64	−40.26	−39.57	−41.84	−40.38	−40.7	−43.75	−41.08	20
Bla (6)	−7.98	−7.68	−7.44	−7.86	−7.88	−7.78	−7.77	−41.57	−41.42	−40.2	−41.79	−42.08	−44.71	−41.96	20.2
Qala Saida (7)	−7.86	−7.51	−7.42	−7.66	−7.7	−7.36	−7.59	−40.64	−39.55	−37.9	−39.28	−38.95	−41.62	−39.65	21
Gullan (8)	−8.16	−7.55	−7.87	−8.1	−8.15	−7.84	−7.95	−42.64	−41.32	−41.1	−41.79	−41.81	−45.02	−42.28	21.3
StD	0.05	0.05	0.06	0.05	0.08	0.11	0.07	0.31	0.33	0.41	0.33	0.63	1.16	0.53	1.6

StD = Analytical standard deviation; NA = Not available; Spring codes can be used to trace the locations of the springs in Figure 1.

4.4.3. Isotopic Pattern of the Karst Springs

The spring water samples have isotopic compositions between −8.29‰ and −6.14‰ for $\delta^{18}O$ and −45.02‰ to −31.89‰ for $\delta^{2}H$ (Table 2). Two regression lines for the karst springs were developed (Figure 6), one for all spring samples, excluding those of November 2012 period ($\delta^{2}H‰ = 2.3‰ + 5.56 \times \delta^{18}O$, R^2 = 0.95, $p < 0.001$ and n = 40), and the other for November 2012 samples ($\delta^{2}H‰ = 5.56 \times \delta^{18}O - 1.36‰$, R^2 = 0.99, $p < 0.001$ and n = 8). The majority of the samples plot between LMWL and MMWL. From this it can be concluded that the precipitation that recharges the karst aquifers originates from Mediterranean vapor masses, reflecting rapid infiltration of rainfall through the karst system and a short transit time (the karst aquifer is shallow, therefore, short residence time does not lead to reliable change in isotopic composition of the recharged water). Shkarta spring

samples are isotopically enriched compared to the other springs. In argillaceous carbonates, evaporation leads to enrichment of isotopes in the pore water [48]. The isotopic enrichment of Shkarta spring relates to slow infiltration because of low permeability in the marly limestone of Shiranish aquifer and thus increased evaporation. The first regression line of the springs (green dashed line in Figure 6) is assumed to be a local evaporation line (LEL), which may occur due to the influence of Shkarta spring. The relation between δ^2H and chloride concentrations of the springs (δ^2H‰ = 21.83‰ + 0.473 × Cl, R^2 = 0.9, and $p < 0.001$) supports the evaporation trend in karst springs of the area (Figure 8a). Minerals like halite (NaCl) react fast with water attaining equilibrium within a short time compared to the residence time of groundwater [49]. Saturation of halite during evaporation of aqueous solution is accompanied by δ^{18}O enrichment [50]. A significant correlation between the *d*-excess and SI_{Halite} is notice (Figure 8b). This plot is interesting and supports the idea of evaporation, because it shows the same evaporation trend of δ^2H-Cl. According to this correlation (Figure 8a), increasing of SI_{Halite} corresponds to decrease in *d*-excess. The correlation between SI_{Halite} and *d-excess* is regarded to the effect of Mediterranean origin of the precipitation in the area of interest. Therefore, the saturation index of halite could represent a tool to evaluate the evaporation process in environmental isotopes of karst waters. The trend of evaporation is increasing from Zewa spring water, which is less enriched with deuterium and chloride, in comparison to Shkarta, which is the most enriched spring (Figure 8).

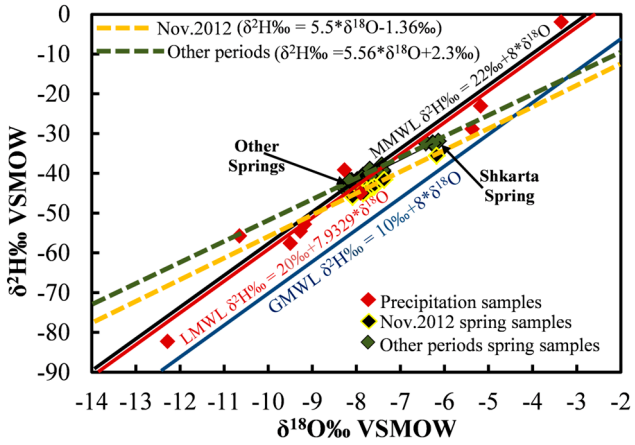

Figure 6. Meteoric water line (LMWL) and springs isotopic line for the studied area. Blue line is the global meteoric water line (GMWL) from [42]; black line is the Mediterranean meteoric water line (MMWL) derived by [43] and the red line is the local meteoric water line (LMWL) from the present study.

4.4.4. Altitude Effect

The isotopic composition of the groundwater in relation to altitude represents an indicator for locating the groundwater recharge area [51,52]. The plots of δ^{18}O and δ^2H in the spring water of the area *versus* the corresponding altitude of the springs are presented in Figure 9. The altitude effect on groundwater of the area is expressed by the linear correlation of δ^{18}O and δ^2H with altitude:

$$\delta^{18}\text{O (‰)} = -6.12 - 0.0017 \times A \quad (4)$$

$$\delta^{2}\text{H (‰)} = -33.24 - 0.008 \times A \quad (5)$$

where A is altitude in meter, R^2 is equal to 0.5 and 0.4, p-value is equal to 0.04 and 0.08 and n is 48 for $\delta^{18}O$ and δ^2H, respectively.

The local isotopic gradient ($LIG_{O\&D}$) shows depletion of stable isotopes by about −0.17‰ and −0.8‰ per 100 m elevation for $\delta^{18}O$ and δ^2H, respectively (Figure 9). The most depleted springs are Zewa, Bla, and Gullan, while Shkarta is the least depleted one (lower elevation).

4.4.5. Temporal Variation

The temporal variation in the isotopic composition of the springs is obvious in all springs (Figure 10). This fluctuation shows more or less the different fingerprints of dry and wet periods. The variation in isotopic composition of karst springs indicates different origins of recharged water and possible connection between the aquifers [53]. The gap between Shkarta and other springs (Figure 10) indicates a connection between Bekhme and Kometan aquifers. Different isotopic signatures for the springs were recognized, separating them into three aquifers: Shiranish aquifer, represented by Shkarta spring (the most enriched isotopes), Kometan aquifer (Sarwchawa and Betwata), mainly represents intermediate isotopic signatures and Behkme aquifer (Zewa, Chewa, Bla, and Gullan springs), generally represented by depleted isotopic signatures if compared with the above two aquifers. The δ^2H is more sensitive to the temporal variation than the oxygen isotope one, because the mean difference ranges from 0.17 to 0.61‰ for $\delta^{18}O$ (about eight times the analytical standard deviation of $\delta^{18}O$, 0.07‰) and from 3.15 to 4.5‰ for δ^2H (about 11 times, 0.4‰). Depletion in δ^2H isotopic signature of the springs was noticed in samples of November 2012 (Figure 7) and this may be due to the nearly lowest recorded temperature of the spring waters during this sampling event and the amount of winter precipitation. This depletion–temperature dependency was also indicated in Figure 7 (lower water temperature characterized by lower $\delta^{18}O$). Depletion was also recorded in Chewa spring for both $\delta^{18}O$ and δ^2H April 2012, which probably occurred by the effect of precipitation amount of rainy season (January to April).

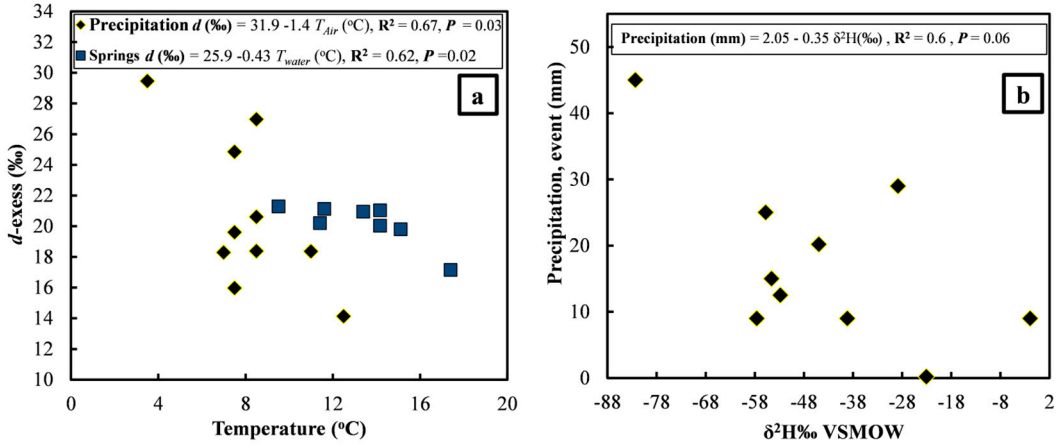

Figure 7. Relation between meteorological and isotopic parameters. (**a**) Plot of d-excess and temperature in precipitation and springs water, data of springs are represents mean d-excess and water temperature of six sampling period for each spring; (**b**) Plot of event precipitation amount and δ^2H in precipitation.

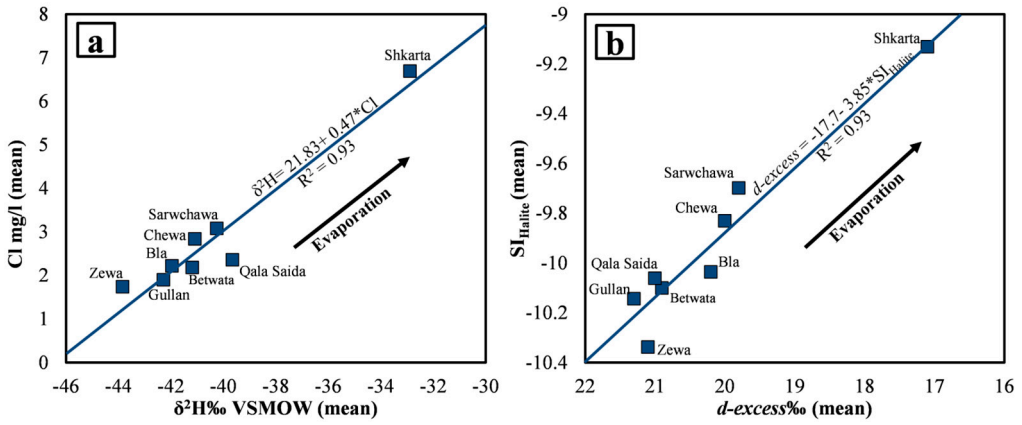

Figure 8. Illustration of evaporation trend from springs of Bekhme aquifer to Shiranish aquifer spring (Shkarta spring). (**a**) δ^2H—chloride plot; (**b**) *d*-excess and SI_{Halite} plot; values of δ^2H, *d-excess*, SI_{Halite} and chloride represent mean values of six samples for each spring: September 2011to September 2012.

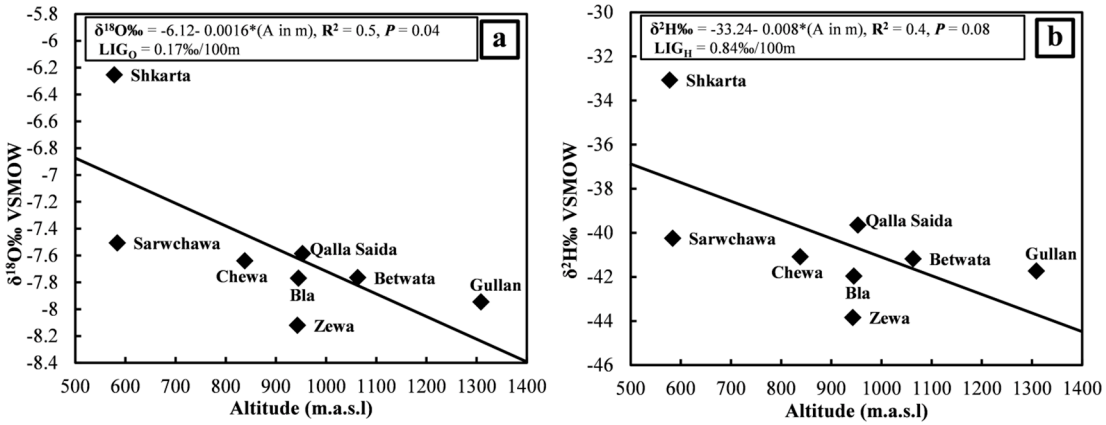

Figure 9. Relation between altitude and $\delta^{18}O$ and δ^2H in the studied area. (**a**) Plot of $\delta^{18}O$ in spring water and altitude of the spring outlet and (**b**) for δ^2H. LIG_O is local isotopic gradient of $\delta^{18}O$ and LIG_H is for δ^2H.

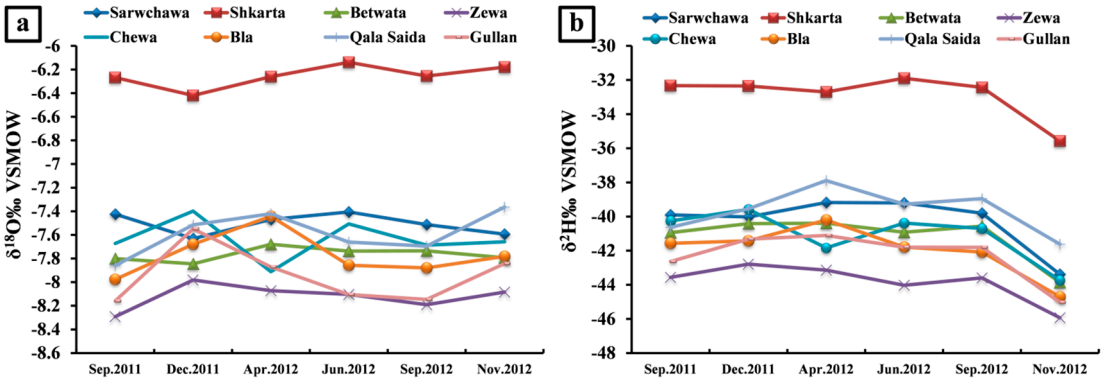

Figure 10. Temporal variation in isotopic composition of the karst springs. (**a**) Variation of $\delta^{18}O$ during the period September 2011 and November 2012; (**b**) Variation of δ^2H during the period September 2011 and November 2012.

4.4.6. Factors Affecting Stable Isotopes in Spring Waters

The water temperature has a significant effect on *d*-excess (*d*-excess‰ = 0.43 × T_{water} (°C) − 25.9, R^2 = 0.6, p = 0.02, n = 48), which shows the same direction as in precipitation and suggests seasonal effects as well (Figure 8a), while air temperature is not significant (*d*-excess‰ = 0.06 × T_{Air} (°C) − 21.4, R^2 = 0.008, p = 0.5, n = 48).

5. Conclusions

The main objective of this study was to understand the isotopic and hydrogeochemical relations in a complex karst system of Makook anticline. EC, pH, Eh, and water temperature temporal variations can be used as tracer for residence time, aquifer storage capacity and depth of the karst aquifers. Hydrogeochemical classification and isotopic composition can be used as indicators for the mean residence time in karst aquifers. The sources of water constituents and driving forces of hydrogeochemical processes are magnified by interrelations of karst water constituents. The sources of the geochemical properties were also indicated by these relations.

The local meteoric water line was derived for the area and is plotting between the global and Mediterranean meteoric water line (however, much closer to the Mediterranean MWL). From the *d*-excess in precipitation, the vapor source was found to be an arid, low humidity, and evaporation-dominant Mediterranean type. Temperature and amount effects are obvious from the isotopic behavior of the precipitation of the area. From the isotopic plot of springs it can be concluded that the recharged precipitation is of Mediterranean origin and that it infiltrates rapidly. Enrichment in stable isotopes gives rise to the hydraulic and hydrodynamic properties of karst aquifers. The local evaporation line is obvious from the oxygen–deuterium plot from Zewa to Shkarta spring and this trend was confirmed by the chloride–deuterium and *d*-excess–SI_{Halite} relations. It can be concluded from the temporal variation of stable isotopes that connections between the aquifers exist.

Acknowledgments

First author is grateful to Diary Ali for his academic guidance. He is thankful to Soran Osman, Kardo Sardar and Ali Wahab for their great support during sampling. First author is also thankful to Lab staff in Chair of Hydrogeology/TU Bergakademie Freiberg for their support during Lab work. The paper has been significantly improved by means of three anonymous reviewers.

Author Contributions

Omed Mustafa developed the project, collected and analyzed the water samples, interpreted the results and wrote the initial manuscript. Broder Merkel and Stephan Weise improved the manuscript and added certain sentences.

Conflict of Interest

The authors declare no conflict of interest.

References

1. Luhmann, A.; Covington, M.; Peters, A.; Alexander, S.; Anger, C.; Green, J.; Runkel, A.C.; Alexander, E. Classification of thermal patterns at karst springs and cave streams. *Ground Water* **2011**, *49*, 324–335.
2. López-Chicano, M.; Bouamama, M.; Vallejos, A.; Pulido-Bosch, A. Factors which determine the hydrogeochemical behaviour of karstic springs. A case study from the Betic Cordilleras, Spain. *Appl. Geochem.* **2001**, *16*, 1179–1192.
3. Liñán Baena, C.; Andreo, B.; Mudry, J.; Carrasco, C.F. Groundwater temperature and electrical conductivity as tools to characterize flow patterns in carbonate aquifers: The Sierra de las Nieves karst aquifer, southern Spain. *Hydrogeol. J.* **2009**, *17*, 843–853.
4. Mawlood, D. Application of Isotope Hydrology Studies Considering the Specific Climate, Hydrogeological and Geological Conditions in Order to Research Underground Water Resources in a Specific Area in the Near East. Ph.D. Thesis, Vienna University of Technology, Vienna, Austria, 2003. (In German)
5. Hamamin, D.; Ali, S. Hydrodynamic study of karstic and intergranular aquifers using isotope geochemistry in Basara basin, Sulaimani, North-Eastern Iraq. *Arab. J. Geosci.* **2013**, *6*, 2933–2940.
6. Al Manmi, D. Water Resources Management in Rania Area, Sulaimaniyah NE-Iraq. Ph.D. Thesis, University of Baghdad, Baghdad, Iraq, 2008.
7. Stevanovic, Z.; Marcovic, M. Hydrogeology of northern Iraq. In *General Hydrogeology and Aquifer System*, 1st ed.; FAO: Rome, Italy, 2004; Volume 2, pp. 42–47.
8. Ministry of Transportation and Communication (MTC). *Directorate of Meteorology and Seismology*; Kurdistan Regional Government: Sulaimani, KR, Iraq, 2012.
9. Jassim, S.Z.; Goff, J.C. *Geology of Iraq*, 1st ed.; Dolin, Prague and Moravian Museum: Prague, Czech Republic, 2006.
10. Bellen, R.C.; Dunnington, H.V.; Wetzel, R.; Morton, D.M.; Dubertret, L. *Stratigraphic Lexicon of Iraq*; Gulf PetroLink: Manama, Bahrain, 2005.
11. Karim, K.H.; Al-Hamadani, R.K.; Ahmad, S.H. Relations between deep and shallow stratigraphic units of Northern Iraq during Cretaceous. *Iran. J. Earth Sci.* **2012**, *4*, 95–103.
12. Sisakian, V. *The Geology of Erbil and Mahabad Quadrangle Sheet NJ-38-14 and NJ-38-15, Scale 1:250 000*; Iraq Geological Survey: Baghdad, Iraq, 1998.
13. Stevanovic, Z.; Iurkiewicz, A.; Maran, A. New insights into karst and caves of Northwestern Zagros (Northern Iraq). *Acta Carsol.* **2009**, *38*, 83–96.
14. APHA. *Standard Methods for the Examination of Water and Wastewater*, 20th ed.; American Public Health Association: Washington, DC, USA, 1998.
15. Parkhurst, D.; Appelo, C. Description of Input and Examples for PHREEQC (Version 3)-A Computer Program for Speciation, Batch-Reaction, One-Dimensional Transport, and Inverse Geochemical Calculations. Available online: http://pubs.usgs.gov/tm/06/a43/pdf/tm6-A43.pdf (accessed on 12 March 2015).
16. Bonacci, O. Analysis of the maximum discharge of karst springs. *Hydrogeol. J.* **2001**, *9*, 328–338.
17. Wood, W. Use and misuse of the chloride-mass balance method in estimating ground water recharge. *Ground Water* **1999**, *37*, 2–3.

18. Scanlon, R.; Healy, W.; Cook, G. Choosing appropriate techniques for quantifying groundwater recharge. *Hydrogeol. J.* **2002**, *10*, 18–39.
19. Bazuhair, S.; Wood, W. Chloride mass-balance method for estimating groundwater recharge in arid areas: Examples from western Saudi Arabia. *J. Hydrol.* **1996**, *186*, 153–159.
20. Marei, A.; Khayat, S.; Weise, S.; Ghannam, S.; Sbaih, M.; Geyer, S. Estimating groundwater recharge using the chloride mass-balance method in the West Bank, Palestine. *Hydrol. Sci. J.* **2010**, *55*, 780–791.
21. Kessler, H. *Water Balance Investigations in the Karst Regions of Hungary*; Act Coll Dubrovnik, AIHS-UNESCO: Paris, France, 1967.
22. Andreo, B.; Vías, J.; Durán, J.; Jiménez, P.; López-Geta, J.; Carrasco, F. Methodology for groundwater recharge assessment in carbonate aquifers: Application to pilot sites in southern Spain. *Hydrogeol. J.* **2008**, *16*, 911–925.
23. Pearson, F.; Scholtis, A. Controls on the chemistry of pore water in a marl of very low permeability. In Proceedings of the 8th International Symposium on Water-Rock Interaction (WRI-8), Vladivostok, Russia, 15–19 August 1995.
24. Parisi, S.; Paternoster, M.; Kohfahl, C.; Pekdeger, A.; Meyer, H.; Hubberten, H.W.; Spilotro, G.; Mongelli, G. Groundwater recharge areas of a volcanic aquifer system inferred from hydraulic, hydrogeochemical and stable isotope data: Mount Vulture, southern Italy. *Hydrogeol. J.* **2011**, *19*, 133–153.
25. Emblanch, C.; Zuppi, G.; Mudry, J.; Blavoux, B.; Batiot, C. Carbon 13 of TIDC to quantify the role of the unsaturated zone: The example of the Vaucluse karst system (southeastern France). *J. Hydrol.* **2003**, *279*, 262–274.
26. Guo, H.; Zhang, B.; Wang, G.; Shen, Z. Geochemical controls on arsenic and rare earth elements approximately along a groundwater flow path in the shallow aquifer of the Hetao Basin, Inner Mongolia. *Chem. Geol.* **2010**, *270*, 117–125.
27. Bundschuh, J. Modeling annual variations of spring and groundwater temperatures associated with shallow aquifer systems. *J. Hydrol.* **1993**, *142*, 427–444.
28. Anderson, M. Heat as a ground water tracer. *Groundwater* **2005**, *43*, 951–968.
29. Vesper, D.; White, W. Storm pulse chemographs of saturation index and carbon dioxide pressure: implications for shifting recharge sources during storm events in the karst aquifer at Fort Campbell, Kentucky/Tennessee, USA. *Hydrogeol. J.* **2004**, *12*, 135–143.
30. Eberts, S.; George, L. *Regional Ground-Water Flow and Geochemistry in the Midwestern Basins and Arches Aquifer System in Parts of Indiana, Ohio, Michigan, and Illinois (Vol. 1423)*; US Geological Survey: Denver, CO, USA, 2000.
31. Al Manmi, D. Chemical and Environmental Study of Groundwater in Sulaimaniyah City and Its Outskirts. Master's Thesis, University of Baghdad, Baghdad, Iraq, 2002.
32. Mustafa, O. Impact of Sewage Wastewater on the Environment of Tanjero River and Its Basin within Sulaimaniyah City, NE Iraq. Master's Thesis, University of Baghdad, Baghdad, Iraq, 2007.
33. Shuster, E.; White, W. Seasonal fluctuations in the chemistry of lime-stone springs: A possible means for characterizing carbonate aquifers. *J. Hydrol.* **1971**, *14*, 93–128.
34. Jacobson, R.; Langmuir, D. Controls on the quality variations of some carbonate spring waters. *J. Hydrol.* **1974**, *23*, 247–265.

35. Raeisi, E.; Karami, G. Hydrochemographs of Berghan karst spring as indicators of aquifer characteristics. *J. Cave Karst Stud.* **1997**, *59*, 112–118.
36. Delbart, C.; Barbecot, F.; Valdes, D.; Tognelli, A.; Fourre, E.; Purtschert; Couchoux, R.; Jean-Baptiste, P. Investigation of young water inflow in karst aquifers using SF6-CFC-3H/ He-85Kr-39Ar and stable isotope components. *Appl. Geochem.* **2014**, *50*, 164–176.
37. Drever, J. The geochemistry of natural waters. In *Surface and Groundwater Environments*, 3rd ed.; Prentice Hall: Upper Saddle River, NJ, USA, 1997; p.436.
38. Chadha, D. A proposed new diagram for geochemical classification of natural waters and interpretation of chemical data. *Hydrogeol. J.* **1999**, *7*, 431–439.
39. Han, D.M.; Liang, X.; Jin, M.G.; Currell, M.J.; Song, X.F.; Liu, C.M. Evaluation of groundwater hydrochemical characteristics and mixing behavior in the Daying and Qicun geothermal systems, Xinzhou Basin. *J. Volcanol. Geotherm. Res.* **2010**, *189*, 92–104.
40. Pavlovskiy, I.; Selle, B. Integrating hydrogeochemical, hydrogeological, and environmental tracer data to understand groundwater flow for a karstified aquifer system. *Groundwater* **2014**, doi:10.1111/gwat.12262.
41. Caetano Bicalho, C.; Batiot-Guilhe, C.; Seidel, L.; van Exter, S.; Jourde, H. Geochemical evidence of water source characterization and hydrodynamic responses in a karst aquifer. *J. Hydrol.* **2012**, *450–451*, 206–218.
42. Craig, H. Isotopic variations in meteoric waters. *Science* **1961**, *133*, 1702–1703.
43. Gat, J.R.; Carmi, I. Evolution of the isotopic composition of atmospheric waters in the Mediterranean Sea area. *J. Geophys. Res.* **1970**, *75*, 3039–3048.
44. Florea, L.J.; McGee, D.K. Isotopic and geochemical variability within shallow groundwater beneath a hardwood hammock and surface water in an adjoining slough (Everglades National Park, Florida, USA). *Isot. Environ. Health Stud.* **2010**, *46*, 190–209.
45. Fröhlich, K.; Gibson, J.J.; Aggarwal, P. Deuterium Excess in Precipitation and Its Climatological Significance. Available online: http://www.iaea.org/inis/collection/NCLCollectionStore/_Public/ 34/017/34017972.pdf (accessed on 12 March 2015).
46. Pang, Z.; Kong, Y.; Fröhlich, K.; Huang, T.; Yuan, L.; Li, Z.; Wang, F. Processes affecting isotopes in precipitation of an arid region. *Tellus B* **2011**, *63*, 352–359.
47. Dansgaard, W. Stable isotopes in precipitation. *Tellus* **1964**, *16*, 460–468.
48. Hamed, Y.; Dhahri, F. Hydro-geochemical and isotopic composition of groundwater, with emphasis on sources of salinity, in the aquifer system in northwestern Tunisia. *J. Afr. Earth Sci.* **2013**, *83*, 10–24.
49. Appelo, C.; Postma, D. *Geochemistry, Groundwater and Pollution*, 2nd ed.; Balkema: New York, NY, USA, 2005; p.683.
50. Pierre, C. Isotopic evidence for the dynamic redox cycle of dissolved sulphur compounds between free and interstitial solutions in marine salt pans. *Chem. Geol.* **1985**, *53*, 191–196.
51. Mazor, I. *Chemical and Isotopic Groundwater Hydrology*, 3rd ed.; M Dekker: New York, NY, USA, 2004; p.352.
52. Dafny, E.; Burg, A.; Gvirtzman, H. Deduction of groundwater flow regime in a basaltic aquifer using geochemical and isotopic data: The Golan Heights, Israel case study. *J. Hydrol.* **2006**, *330*, 506–524.

53. Kattan, Z. Environmental isotope study of the major karst springs in Damascus limestone aquifer systems: Case of the Figeh and Barada springs. *J. Hydrol.* **1997**, *193*, 161–182.